ARTICLES

Dye-Sensitized TiO_2 Solar Cells: Structural and Photoelectrochemical Characterization of Nanocrystalline Electrodes Formed from the Hydrolysis of $TiCl_4$

N.-G. Park, G. Schlichthörl, J. van de Lagemaat, H. M. Cheong, A. Mascarenhas, and A. J. Frank*

National Renewable Energy Laboratory, 1617 Cole Boulevard, Golden, Colorado 80401

Received: November 24, 1998; In Final Form: March 1, 1999

The structure and photoelectrochemical properties of TiO_2 films deposited onto SnO_2 conducting glass from the ambient hydrolysis of $TiCl_4$ and annealed at temperatures ranging from 100 to 500 °C were studied by Raman spectroscopy, X-ray diffraction (XRD), transmission electron microscopy (TEM), intensity-modulated photovoltage spectroscopy (IMVS), and intensity-modulated photocurrent spectroscopy (IMPS) measurements. Analysis of the XRD and Raman spectra shows that $TiCl_4$-produced TiO_2 films have the rutile structure, regardless of annealing temperature. The TEM reveals that the rutile TiO_2 films consist of rod-shaped particles that grow with increasing annealing temperature. The AM-1.5 short-circuit photocurrent J_{sc} and open-circuit photovoltage V_{oc} of Ru[LL′(NCS)$_2$]-sensitized (L = 2,2′-bypyridyl-4,4′-dicarboxylic acid, L′ = 2,2′-bipyridyl-4,4-ditetrabutylammoniumcarboxylate) 4.5 μm thick rutile films increase significantly with annealing temperature, from 1.1 mA/cm^2 and 602 mV at 100 °C to 8.7 mA/cm^2 and 670 mV at 500 °C. Studies of the incident photon-to-current conversion efficiency (IPCE), the photocurrent−voltage characteristics, the optical appearance, the water content, and the particle size of the films indicate that the increase of both J_{sc} and V_{oc} with annealing temperature is due, in part, to increased dye adsorption resulting from the evaporation of surface water and the improved light-scattering properties of the film associated with the growth of rutile particles. IMVS and IMPS measurements indicate that variations of the charge-collection efficiency of the cell, which increases from 86% for the 300 °C annealed samples to above 99% for the 500 °C annealed samples, have only a minor effect on J_{sc}. Analysis of the time constants at open circuit and short circuit for a given electron injection current suggests that the ratio of free-to-trapped electrons at short circuit decreases and the diffusion coefficient of free electrons increases with annealing temperature. Raman and XRD measurements and other observations indicate that treating transparent nanocrystalline anatase TiO_2 electrodes with $TiCl_4$ produces a translucent overlayer of rutile TiO_2. The increased film thickness and light-scattering characteristics of the rutile overlayer may explain, in part, the improved IPCE observed for dye-sensitized $TiCl_4$-treated nanocrystalline anatase TiO_2 electrodes.

Introduction

Regenerative photoelectrochemical solar cells based on photosensitization of nanocrystalline TiO_2 are regarded as a potential low-cost alternative to conventional solid-state devices.[1] Solar-to-electrical energy conversion efficiencies as high as 10−11% at AM 1.5 have been reported.[2−4] To achieve high cell efficiency, much research has been directed toward improving the photocurrent and photovoltage by, for example, developing new sensitizers,[5−19] increasing the light-scattering properties of the film,[20,21] suppressing charge recombination,[2,22] improving the interfacial energetics,[23] and altering the particle morphology.[3,24,25]

Surface treatment of dye-sensitized TiO_2 electrodes with organic molecules, such as pyridines[2,22] and ammonia,[23] has been shown to improve substantially the cell photovoltage. Intensity-modulated photovoltage spectroscopy IMVS studies[23] have shown that the improved photovoltage is a direct result of band edge movement caused by these reagents deprotonating the partially protonated TiO_2 particles. Improved photocurrent has resulted from exposing nanocrystalline anatase TiO_2 electrodes to a hydrolyzed $TiCl_4$ solution.[3] Although the mechanism for the improved photocurrent was not examined, it was hypothesized that $TiCl_4$ treatment increases the necking between particles of the film, thus facilitating the percolation of photoinjected electrons from one particle to another and lowering the probability of recombination. No structural information of $TiCl_4$-treated films was provided.

In this article, we examine the influence of annealing temperature on the crystal structure, particle size, and particle morphology of TiO_2 films deposited onto SnO_2 conducting glass from the ambient hydrolysis of $TiCl_4$. The photocurrent−voltage $J-V$ properties of the annealed films are compared. Intensity-modulated photovoltage spectroscopy IMVS[23,26] and intensity-modulated photocurrent spectroscopy IMPS[26−30] are used to measure the respective time constants for charge recombination at open circuit and the combined processes of charge collection

10.1021/jp984529i CCC: $18.00
Published on Web 04/09/1999

and charge recombination at short circuit in Ru[LL′$(NCS)_2$]-sensitized (L = 2,2′-bypyridyl-4,4′-dicarboxylic acid, L′ = 2,2′-bipyridyl-4,4-ditetrabutylammoniumcarboxylate) $TiCl_4$-produced TiO_2 films. The structural composition of $TiCl_4$-treated nanocrystalline anatase TiO_2 electrodes was also studied.

Experimental Section

Conducting glass plates (1.2 × 1.25 cm; Asahi Glass Co.; F-doped SnO_2 overlayer, 75% transmittance in the visible, 5% haze, 5 Ω/sq) were used as the substrate for depositing nanocrystalline TiO_2 films from the ambient hydrolysis of $TiCl_4$. To deposit a film, a bare or an anatase TiO_2-coated conducting glass plate was immersed into a 0.2 M $TiCl_4$ (Aldrich) aqueous solution in a closed, air-filled chamber for 2 days. The electrodes were then rinsed with distilled water and annealed at a temperature of 100, 300, or 500 °C for 30 min. The thickness of the resulting TiO_2 film was 4.5 ± 0.5 μm as measured with a Tencor Alpha-step profiler. An anatase TiO_2 colloidal solution, consisting of 15−20 nm sized particles, was prepared by the hydrolysis of titanium tetraisopropoxide in the presence of acetic acid, followed by autoclaving at 230 °C for 12 h;[31] the particle size was determined by transmission electron microscopy TEM (Philips CM30). Transparent nanocrystalline anatase TiO_2 films were deposited onto conducting glass substrates from the resulting colloidal solution as detailed elsewhere.[22] In some cases, the anatase films were treated with $TiCl_4$ under the conditions described above and then annealed at 500 °C for 30 min.

For photosensitization studies, the TiO_2 electrodes were soaked in absolute ethanol containing 5 × 10^{-4} M Ru[LL′$(NCS)_2$] (L = 2,2′-bypyridyl-4,4′-dicarboxylic acid, L′ = 2,2′-bipyridyl-4,4′-ditetrabutylammoniumcarboxylate) for 24 h at room temperature. The dye-covered electrodes were then rinsed with absolute ethanol and dried under a N_2 stream. A second plate of glass, covered with platinum, was placed over the $TiCl_4$-produced TiO_2 film, and the edges of the cell were sealed with a plastic resin as described elsewhere.[23] The redox electrolyte was composed of 0.8 M 1,2-dimethyl-3-hexyl imidazolium iodide and 50 mM I_2 in acetonitrile. The 1,2-dimethyl-3-hexyl imidazolium iodide was synthesized as detailed in the literature,[32] and its structure was confirmed by ^{1}H NMR.

The Raman spectra were taken in the backscattering geometry using the 514.5 nm line of an Ar ion laser as the excitation source. The signal was dispersed by a Spex 0.6 m triple spectrometer and detected with a liquid nitrogen cooled high-resolution charge coupled device detector array. Both the spectral resolution and the accuracy of the Raman shift are estimated to be ∼2 cm^{-1}. X-ray diffraction XRD measurements were performed with Cu Kα radiation (λ = 1.5406 Å) using a SCINTAG DMS-2000. The TiO_2 film morphology and particle size were measured by TEM. Samples for TEM measurements were prepared by scraping a small amount of powder from the films into ethanol and then dispersing it via an ultrasonic bath; the resulting suspension was deposited onto a carbon-coated copper grid. Thermogravimetric analysis (TGA) was conducted with a computer-controlled TGA 51 thermogravimetric analyzer (TA Instruments); the temperature was increased at a rate of 10 °C/min, and samples were exposed to a continuous stream of nitrogen.

Photocurrent−voltage $J-V$ measurements were performed using a Keithley model 236 source measure unit. A 1000 W sulfur lamp (Fusion Lighting Inc.) served as a light source, and its light intensity (or radiant power) was adjusted with a Si solar cell equipped with a KG-5 filter (Schott) for approximating AM-1.5 radiation. The light source for the incident photon-to-current conversion efficiency (IPCE) measurements was a 150 W quartz halogen lamp equipped with a Photon Technology International model 1492 monochromator. The intensity was measured with a UDT Instrument model S370 optometer and a UDT instrument model 221 calibrated photodiode. The setup for IMVS measurements is described elsewhere.[23] For IMPS measurements, a SR 570 current preamplifier (Stanford Research Systems) was used for the current to voltage conversion; both IMVS and IMPS measurements were performed on the same electrodes.

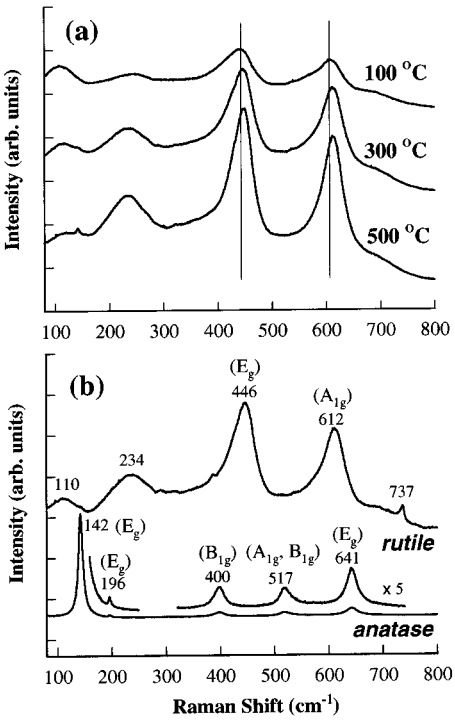

Figure 1. Raman spectra of (a) TiO_2 films deposited onto conducting glass from the hydrolysis of $TiCl_4$ and annealed at various temperatures and (b) reference rutile and anatase TiO_2 films.

Results and Discussion

Structure of the TiO_2 Films. Figure 1 compares the Raman spectra of TiO_2 deposited films annealed at 100, 300, and 500 °C with reference spectra for rutile and anatase crystalline TiO_2. The $TiCl_4$-produced TiO_2 films crystallize as rutile regardless of annealing temperature. Suspensions and colloidal solutions of rutile can also be formed from the hydrolysis of $TiCl_4$ under other conditions.[33]

As the annealing temperature of the films increases, the respective energies of the E_g band and the A_{1g} band increase from 439 cm^{-1} (100 °C) to 446 cm^{-1} (300 and 500 °C) and from 607 cm^{-1} (100 °C) to 611 cm^{-1} (300 and 500 °C), and the line width of the bands narrows. In addition, the 240 cm^{-1} band gains intensity, while the band at about 110 cm^{-1} disappears gradually. Both the shift to higher energy and the line width narrowing of the E_g and A_{1g} bands are associated with an increased crystallite size[34,35] induced by heating of the films. The presence of the band at 234 cm^{-1} indicates the occurrence of either disorder-induced scattering[35−37] or second-order scattering.[38] The increased intensity of the band with the annealing temperature suggests a temperature-induced lattice disorder. Although the broad band at about 110 cm^{-1} is not present in the spectrum of single crystalline rutile, it is observed in the spectrum of nanocrystalline rutile synthesized hydrothermally from the hydrolysis of $TiCl_4$.[34] The lower intensity of

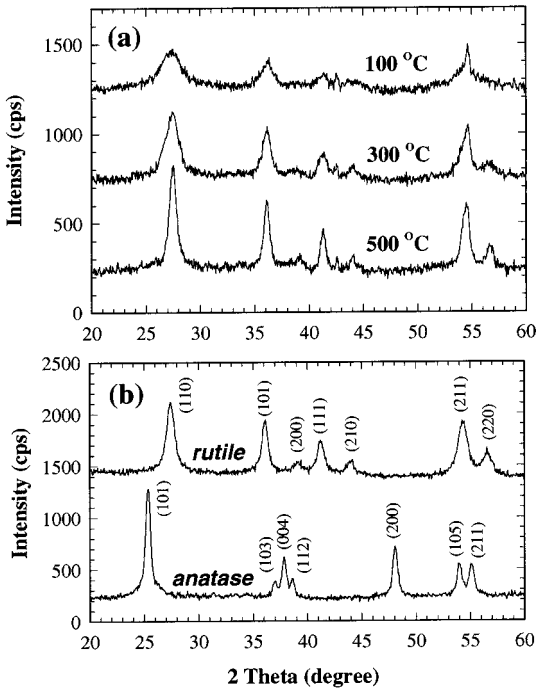

Figure 2. X-ray diffraction patterns of (a) TiO_2 films deposited onto conducting glass from the hydrolysis of $TiCl_4$ and annealed at various temperatures and (b) reference rutile and anatase TiO_2 films.

the 110 cm^{-1} band with increasing annealing temperature is consistent with crystallite growth.[34]

Figure 2 shows XRD patterns of TiO_2 deposited films, along with reference data for rutile and anatase TiO_2. An excellent match of the diffraction pattern of $TiCl_4$-produced TiO_2 films with the rutile reference data confirms the identity of the films by Raman spectroscopy. Moreover, a comparison of the area under the 110 cm^{-1} peak of $TiCl_4$-produced TiO_2 films indicates that the amount of nanocrystalline rutile present in the film was essentially the same at each annealing temperature. Also, it can be seen that the peaks become sharper with increasing annealing temperature. Such behavior, according to the Scherrer equation [$L = 0.9\lambda/B(2\theta)\cos\theta$, where L is the crystallite size and $B(2\theta)$ is the line width] is indicative of crystallite growth, which agrees with the Raman studies.

Figure 3 shows TEM micrographs of the $TiCl_4$-produced TiO_2 films annealed at 100, 300, and 500 °C. The rutile TiO_2 films consists of rod-shaped particles that grow with increasing annealing temperature; the observed particle growth with temperature concurs with Raman and XRD results. The typical size of the particles (diameter × length) increases from 3 × 20 nm at 100 °C to 9 × 40 nm at 300 °C to 15 × 75 nm at 500 °C. The increase of particle size for a fixed amount of nanocrystalline rutile (see discussion of XRD above) indicates that the area-to-volume ratio declines with increasing annealing temperature. The roughness factor of the films (geometric area/real area), estimated from the particle shape and size and the film thickness (4.5 μm) and porosity ($P = 0.3$),[39] decreases from 4200 at 100 °C to 1400 at 300 °C to 840 at 500 °C. Within experimental error, the film thickness did not vary with annealing temperature; for a fixed thickness and quantity of rutile, the film porosity is expected to be independent of annealing temperature. The presence of lattice fringes (Figure 3b,d,f) is indicative of crystallized particles. The selected area electron diffraction pattern of the 500 °C annealed sample in Figure 4 displays the crystallographic faces of rutile TiO_2.

Photocurrent−Voltage Characteristics. Figure 5 and Table 1 show that the $J-V$ characteristics of Ru[LL′$(NCS)_2$]-sensitized

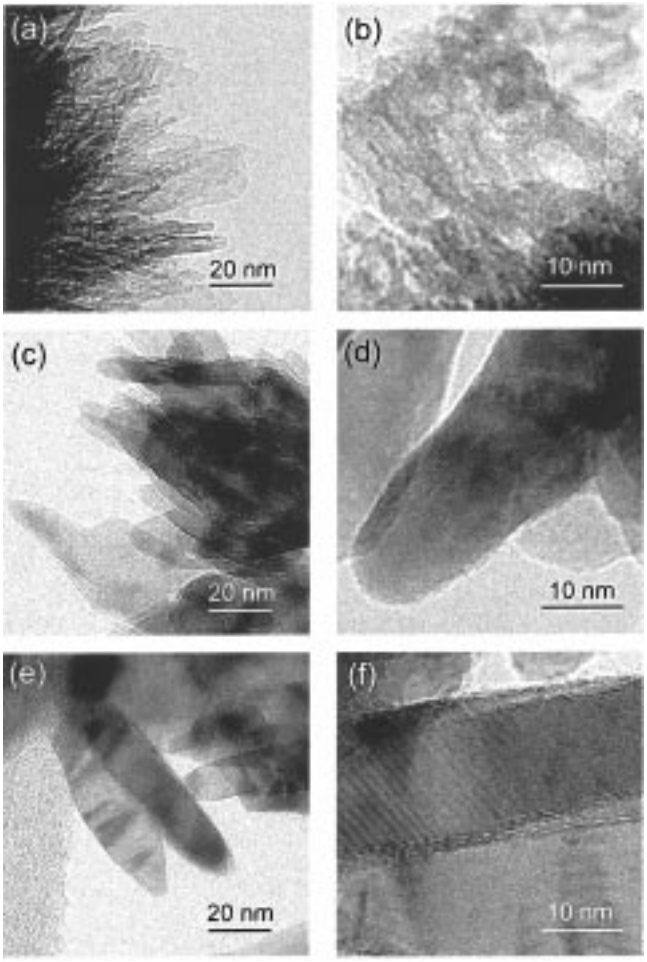

Figure 3. TEM micrographs of $TiCl_4$-produced TiO_2 films annealed at (a),(b) 100 °C, (c),(d) 300 °C, and (e),(f) 500 °C.

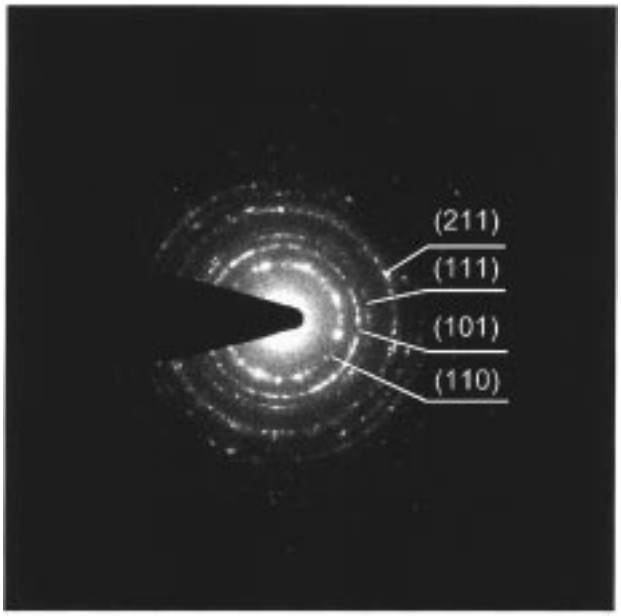

Figure 4. Selected area electron diffraction pattern of a $TiCl_4$-produced TiO_2 film annealed at 500 °C.

nanocrystalline rutile TiO_2 electrodes improve with annealing temperature. The J_{sc} increases from 1.1 to 8.7 mA/cm^2 as the annealing temperature of the film increases from 100 to 500 °C. With higher annealing temperatures, the TiO_2 films become more intensely red and the absorbance of the dye increases,

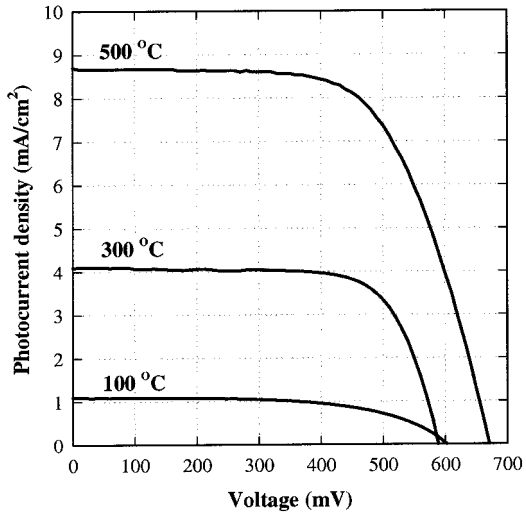

Figure 5. *J*−*V* curves of Ru[LL′(NCS)$_2$]-sensitized nanocrystalline rutile TiO_2 electrodes. The TiO_2 films were annealed at 100, 300, and 500 °C. The redox electrolyte contained 1,2-dimethyl-3-hexyl imidazolium iodide (0.8 M) and iodine (50 mM) in acetonitrile; the radiant power is 100 mW/cm^2 (AM 1.5).

TABLE 1: Effect of Annealing Temperature on Photocurrent−Voltage (*J*−*V*) Characteristics of Ru[LL′(NCS)$_2$]-Sensitized Nanocrystalline Rutile TiO_2 Films[a,b]

annealing temperature (°C)	J_{sc} (mA/cm^2)	V_{oc} (mV)	*FF*	(%)
100	1.09	602	0.59	0.39
300	4.10	589	0.72	1.74
500	8.70	671	0.64	3.74

[a] Radiant power is 100 mW/cm^2 (AM 1.5). [b] Redox electrolyte contained 0.8 M 1,2-dimethyl-3-hexyl imidazolium iodide and 50 mM iodine in acetonitrile.

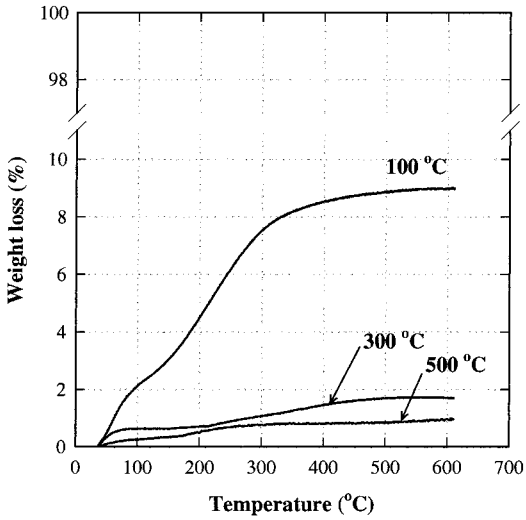

Figure 6. TGA curves of $TiCl_4$-produced rutile TiO_2 films annealed at (a) 100 °C, (b) 300 °C, and (c) 500 °C.

indicating that the adsorbed dye concentration also increases with the annealing temperature. The dependence of adsorbed dye concentration on annealing temperature can be understood from TGA measurements. Figure 6 shows that the water content of a TiO_2 film diminishes significantly with annealing temperature, indicating that samples annealed at 100 °C retain much more water than samples annealed at higher temperatures. Furthermore, most of the water loss from the 100 and 300 °C annealed samples occurs over the temperature range of about

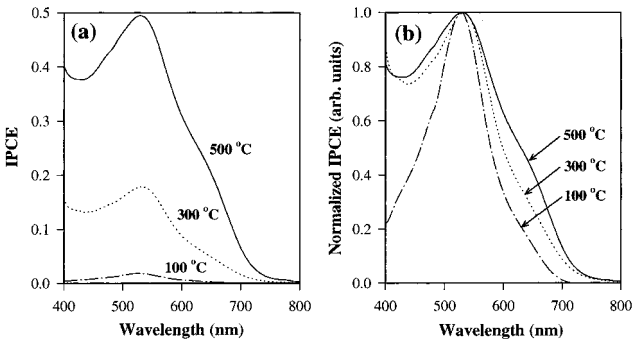

Figure 7. Dependence of the (a) absolute and (b) normalized values of the IPCE on wavelength for Ru[LL′(NCS)$_2$]-sensitized nanocrystalline rutile TiO_2 electrodes. The TiO_2 films were annealed at 100, 300, and 500 °C. The redox electrolyte contained 1,2-dimethyl-3-hexyl imidazolium iodide (0.8 M) and iodine (50 mM) in acetontrile. No correction was made for reflection losses.

40−300 °C; the 500 °C annealed samples showed no significant water loss after 200 °C. The evaporation of water is presumed to arise from the loss of interstitial and adsorbed water and from the dehydroxlation/depronation of the TiO_2 surface. Similar observations have been reported by others.[40] The loss of water from TiO_2 films with annealing temperature may be associated with an increase of available surface sites for dye adsorption. However, the possible effect of a surface layer of amorphous Ti oxides and hydroxides on dye adsorption cannot be ruled out; heating of such a layer would convert it to the rutile phase and drive off water. The change of adsorption characteristics of the TiO_2 particles with annealing temperature may also affect the electron injection efficiency of the dye. In addition to the increased amount of adsorbed dye, the light-harvesting efficiency of the film is expected to benefit from the growth of crystallites with annealing temperature as a result of the improved internal light-scattering characteristics of the film.[21]

Figure 7a displays the monochromatic incident photon-to-current conversion efficiency (IPCE) as a function of wavelength measured at short circuit; no correction was made for reflection losses from the cell. The IPCE can be expressed theoretically as the product of the light absorption efficiency of the dye, the quantum yield of electron injection, and the efficiency of collecting the injected electrons at the conducting glass substrate. Figure 7b shows the same IPCE data normalized to the intensity of the 540 nm peak. Following the same trend observed in Figure 5, the IPCE increases significantly with the annealing temperature of the film, which correlates with the increased amount of adsorbed dye. The comparatively low IPCE values of the 100 °C annealed sample at the high- and low-energy side of the peak maximum in Figure 7b is attributed to the relatively low dye concentration (poor light absorption by the film). Also, with less light absorption by the dye in the 400−500 nm spectral region, light absorption by iodide species (I_3^-) in the electrolyte is accentuated. The low IPCE values of the 100 °C annealed sample at long wavelength (600−800 nm) may also be due to the presence of comparatively smaller rutile particles and consequently the less effective light-scattering characteristics of the film.[41]

IMVS and IMPS. Figure 8 shows a plot of the photoinduced charge Q_{oc} vs V_{oc} at different annealing temperatures of the films; Q_{oc} is calculated[23] as the product of the time constant at open circuit τ_{oc} (see Figure 9a) and J_{sc}. For the same V_{oc}, the photoinduced charge of the 100 °C annealed samples is much less than that of the 300 °C and 500 °C annealed samples. The photocapacitance of the 100 °C annealed samples (dQ_{oc}/dV = 2.5 to 3.0 μF/cm^2) is close to the value of the Helmholtz

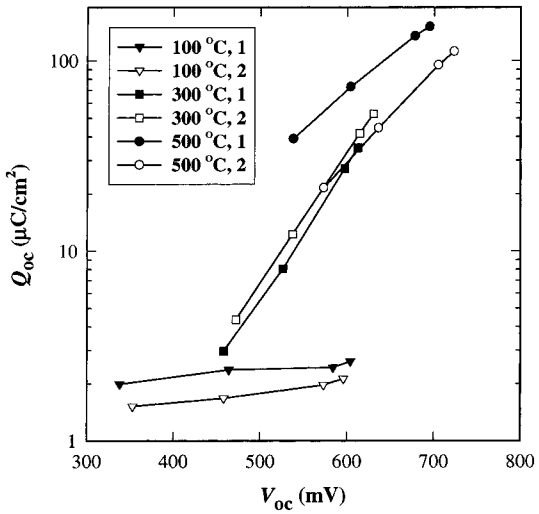

Figure 8. Dependence of calculated charge ($Q_{oc} = J_{sc}\tau_{oc}$) on V_{oc} for Ru[LL′(NCS)$_2$]-sensitized nanocrystalline rutile TiO_2 electrodes. Two sample sets (1,2) of TiO_2 films were annealed at 100, 300, and 500 °C. The redox electrolyte contained 1,2-dimethyl-3-hexyl imidazolium iodide (0.8 M) and iodine (50 mM) in acetontrile. J_{sc} equals the charge injection current into TiO_2, and τ_{oc} is the IMVS-measured time constant at open circuit.

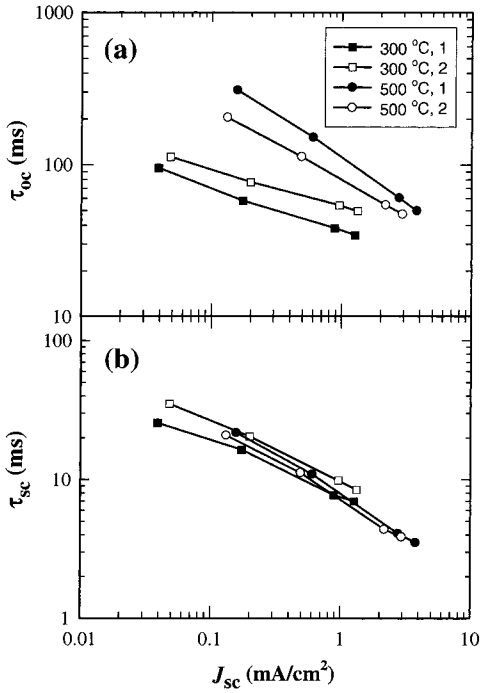

Figure 9. Relation of (a) the IMVS-measured time constant at open circuit τ_{oc} and (b) the IMPS-measured time constant at short circuit τ_{sc} to the light intensity represented by J_{sc} for Ru[LL′(NCS)$_2$]-sensitized nanocrystalline rutile TiO_2 electrodes. Two sample sets (1,2) of TiO_2 films were annealed at 300 and 500 °C. The redox electrolyte contained 1,2-dimethyl-3-hexyl imidazolium iodide (0.8 M) and iodine (50 mM) in acetontrile.

capacitance of the conducting glass/redox electrolyte interface,[23] suggesting that the measured charge is located mainly on the conducting glass. The photocapacitance of the conducting glass is not expected to change markedly with the annealing temperature. In the case of the 300 and 500 °C annealed samples, the light-induced charge is located principally in the TiO_2 film. For the same V_{oc}, the photoinduced charge of the 500 °C annealed samples is larger than that of the 300 °C annealed samples. The inverse of the slope of the ln Q_{oc} vs V_{oc} plot is indicative of whether the photoinduced charge resides in the conduction band or in trap states.[23] If the charge is located principally in the conduction band, the predicted $dV_{oc}/d\ln Q_{oc}$ is 26 mV. If $dV_{oc}/d\ln Q_{oc}$ is much larger than 26 mV, the charge resides predominantly in traps. Because $dV_{oc}/d\ln Q_{oc}$ for the higher temperature annealed samples (63 mV for 300 °C and 100 mV for 500 °C) is much larger than 26 mV, it may be deduced that the charge is located predominantly in traps. Furthermore, because the 500 °C annealed samples have a larger Q_{oc} than the 300 °C annealed samples, it follows that the former samples have a higher density of trapped electrons at a given V_{oc} and light intensity. The annealing process can introduce trap states with energies in the vicinity of the Fermi level. From the ln Q_{oc} vs V_{oc} plot, one cannot distinguish whether these traps (e.g., oxygen deficiencies) are in the bulk or at the surface. However, in view of the large surface-area-to-volume ratio of the nanocrystalline films, one expects that the traps are located primarily at the surface. The inverse of the slope of the ln J_{sc} vs V_{oc} plot indicates whether the recombination occurs predominantly via the conduction band or via trap states.[23] If recombination occurs via the conduction band, $dV_{oc}/d\ln J_{sc}$ equals 26 mV. If $dV_{oc}/d\ln J_{sc}$ is much larger than 26 mV, recombination takes place via traps. From the analysis of the ln J_{sc} vs V_{oc} plots ($dV_{oc}/d\ln J_{sc} \approx 48$ mV; not shown) for the high-temperature annealed films, it is inferred that recombination occurs predominantly via traps. These results thus imply that in the 300 and 500 °C annealed samples that recombination at open circuit takes place principally via surface traps. In contrast, most of the recombination in the 100 °C annealed samples is expected to occur at the conducting glass surface. Figure 9a shows the time constant at open circuit τ_{oc} as a function of J_{sc} for the 300 and 500 °C annealed samples. (The data for the 100 °C annealed samples are omitted because recombination occurs predominantly on the conduction glass surface and not on the TiO_2 surface as discussed above.) It can be seen that for a given short circuit photocurrent, τ_{oc} of the 500 °C annealed sample is larger than that of the 300 °C annealed sample, indicating that the time constant for surface recombination becomes slower with increased annealing temperature. The larger time constant for surface recombination is expected to promote an increase of V_{oc} (Figure 5). Figure 9b shows the dependence of the time constant at short circuit τ_{sc}, corresponding to the combined processes of electron transport (charge collection) and recombination, on J_{sc}. At short circuit, the time constant depends on the ratio of free-to-trapped electrons and on the diffusion coefficient of electrons in the conduction band. Thus, τ_{sc} is influenced by the total number of surface states in the film, the position of the Fermi level, and the electrical connectivity of the TiO_2 network. A comparison of parts a and b of Figure 9 reveals that τ_{sc} is smaller than τ_{oc} at the same J_{sc}, implying that the total amount of charge in the film at short circuit ($Q_{sc} \propto \tau_{sc} J_{sc}$) is lower than the total amount of charge in the film at open circuit ($Q_{oc} = \tau_{oc} J_{sc}$). Furthermore, Figure 9b shows that both the 300 and 500 °C annealed samples contain comparable amounts of charge at a given J_{sc} at short circuit. Assuming that trapping and detrapping of electrons are much faster than electron transport,[26] these results imply that the filling up of surface states of the 500 °C annealed samples occurs at a lower energy (or Fermi level) than that of the 300 °C annealed samples at the same J_{sc} or electron injection current J_{inj} (see J_{inj} discussion below). In turn, this suggests that the ratio of free-to-trapped electrons in the 500 °C annealed samples is lower than that of the 300 °C annealed samples at the same J_{inj}. Because the 300 and 500 °C annealed samples have comparable values of τ_{sc} at a given J_{sc} (Figure 9b), the diffusion coefficient

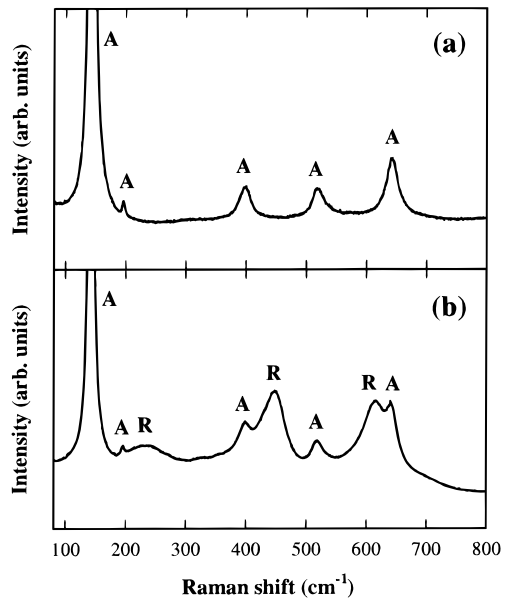

Figure 10. Raman spectra of nanocrystalline anatase TiO_2 electrode (a) before and (b) after exposure to the hydrolysis of $TiCl_4$. The letters A and R denote the anatase and rutile phases, respectively.

of electrons in the TiO_2 film of the 500 °C annealed samples must be larger than that of the 300 °C annealed samples. Hence, increasing the temperature of the sintering process improves the transport of electrons through the nanocrystalline rutile TiO_2 films.

The charge-collection efficiency at short circuit (η) can be estimated from the relation[26]

$$\eta = 1 - \left(\frac{\tau_{oc}}{1.2\tau_{sc}}\right)^{-m_1/0.9} \quad (1)$$

where τ_{oc} and τ_{sc} are obtained from IMVS and IMPS measurements, respectively, and the parameter m_1 is determined from the slope of a ln J_{sc} vs ln Q_{oc} ($Q_{oc} = J_{sc}\tau_{oc}$) plot. The charge-collection efficiency is about 86% for the 300 °C annealed samples and is above 99% for the 500 °C annealed samples; both values of η do not depend significantly on the light intensity. The increased charge-collection efficiency (eq 1) of the 500 °C annealed samples is attributed to a larger time constant for recombination τ_{oc}. (Note: the charge-collection efficiency of the 100 °C annealed sample cannot be estimated from eq 1 because recombination occurs predominantly at the conducting glass surface and not at the TiO_2 surface.) The small difference (14%) between the charge-collection efficiency of the 300 °C annealed samples (86%) and the 500 °C annealed samples (>99%) is not sufficient to explain the factor of 2−3 difference between their respective J_{sc} (Figure 5) and IPCE (Figure 7a). Furthermore, because the charge-collection efficiencies of the 300 and 500 °C annealed samples do not differ markedly, it implies that the electron injection current J_{inj} is approximately the same as J_{sc} ($J_{inj} = J_{sc}/\eta$).

$TiCl_4$-Treated Nanocrystalline Anatase TiO_2 Electrodes. $TiCl_4$ treatment of transparent nanocrystalline anatase TiO_2 electrodes increases the thickness of the TiO_2 films from 9 to 13 μm. A comparison of the Raman spectra of nanocrystalline anatase TiO_2 films before and after $TiCl_4$ treatment (Figure 10) shows that the $TiCl_4$-treated electrode is composed of a mixture of anatase and rutile; the presence of the rutile phase was confirmed by XRD (not shown). Furthermore, depositing the rutile TiO_2 overlayer onto the transparent nanocrystalline anatase film alters the light-scattering property of the resulting film, causing it to become translucent. Both the increased film thickness and the enhanced light-scattering characteristics of the film may explain, in part, the improved IPCE reported[3] for dye-sensitized $TiCl_4$-treated nanocrystalline anatase TiO_2 electrodes.

Conclusions

Raman spectroscopy, XRD, and TEM studies show that TiO_2 films deposited onto conducting glass from the hydrolysis of $TiCl_4$ consist of rod-shaped nanocrystallites having the rutile structure, regardless of annealing temperature over the range 100−500 °C. The increased short-circuit photocurrent of the dye-sensitized rutile TiO_2 electrodes with the annealing temperature correlates with an increased concentration of adsorbed dye and improved light-scattering properties of the film associated with the growth of rutile particles. Variations of the charge-collection efficiency of the film, which shows a small increase with the annealing temperature, have only a minor effect on the photocurrent. Analysis of the time constants at open circuit and short circuit at a given electron injection current suggests that the ratio of free-to-trapped electrons at short circuit decreases and the diffusion coefficient of free electrons increases with annealing temperature. The increase of V_{oc} with annealing temperature at a given J_{sc} is due, in part, to an increased light-harvesting efficiency and a longer time constant for surface recombination. Treating transparent nanocrystalline anatase TiO_2 electrodes with $TiCl_4$ produces an overlayer of rutile, which increases the thickness of the overall TiO_2 film and improves its visible-to-near-infrared light-scattering properties. These attributes are expected to promote high photocurrent and may account for the improved incident photon-to-current conversion efficiency observed for dye-sensitized $TiCl_4$-treated nanocrystalline anatase TiO_2 electrodes.

Acknowledgment. We are grateful to Dr. Michael Grätzel at the Swiss Federal Institute of Technology Lausanne for providing the dye and to Mr. Kazuo Sato at the Asahi Glass Co. and Dr. Yuji Muraoka at Tohuku University for providing the conducting glass. This work was supported by the Office of Science, Division of Chemical Sciences (G.S., J.v.d.L., and A.J.F.), and the Office of Utility Technologies, Division of Photovoltaics (N.-G. Park), U.S. Department of Energy, under Contract DE-AC36-83CH10093.

References and Notes

(1) O'Regan, B.; Grätzel, M. *Nature* **1991**, *353*, 737.
(2) Nazeeruddin, M. K.; Kay, A.; Rodicio, I.; Humphry-Baker, R.; Müller, E.; Liska, P.; Vlachopoulos, N.; Grätzel, M. *J. Am. Chem. Soc.* **1993**, *115*, 6382.
(3) Barbe, C. J.; Arendse, F.; Comte, P.; Jirousek, M.; Lenzmann, F.; Shklover, V.; Grätzel, M. *J. Am. Ceram. Soc.* **1997**, *80*, 3157.
(4) Green, M. A.; Emery, K.; Bucher, K.; King, D. L.; Igari, S. *Prog. Photovolt. Res. Appl.* **1998**, *6*, 35.
(5) Kay, A.; Grätzel, M. *J. Phys. Chem.* **1993**, *97*, 6272.
(6) Bignozzi, C. A.; Argazzi, R.; Indelli, M. T.; Scandola, F. *Sol. Energy Mater. Sol. Cells* **1994**, *32*, 229.
(7) Argazzi, R.; Bignozzi, C. A.; Heimer, T. A.; Castellano, F. N.; Meyer, G. J. *Inorg. Chem.* **1994**, *33*, 5741.
(8) Grätzel, M.; Fraser, D.; Zakeeruddin, S. M.; Nazeeruddin, M. K. U.S. Patent 5 393 903, 1995.
(9) Heimer, T. A.; D'Arcangelis, S. T.; Frazad, F.; Stipkala, J. M.; Meyer, G. J. *Inorg. Chem.* **1996**, *35*, 5319.
(10) Yanagi, H.; Chen, S.; Lee, P. A.; Nebesny, K. W.; Armstrong, N. R.; Fujishima, A. *J. Phys. Chem.* **1996**, *100*, 5447.
(11) Nazeeruddin, M. K.; Péchy, P.; Grätzel, M. *Chem. Commun.* **1997**, 1705.
(12) Nazeeruddin, M. K.; Müller, E.; Humphry-Baker, R.; Vlachopoulos, N.; Grätzel, M. *J. Chem. Soc., Dalton Trans.* **1997**, 4571.

(13) Zakeeruddin, S. M.; Nazeeruddin, M. K.; Péchy, P.; Rotzinger, F. P.; Humphry-Baker, R.; Kalyanasundaram, K.; Grätzel, M.; Shklover, V.; Haibach, T. *Inorg. Chem*. **1997**, *36*, 5937.

(14) Ruile, S.; Kohle, O.; Péchy, P.; Grätzel, M. *Inorg. Chim. Acta* **1997**, *261*, 129.

(15) Meyer, G. J. *J. Chem. Educ*. **1997**, *74*, 652.

(16) He, J.; Zhao, J.; Shen, T.; Hidaka, H.; Serpone, N. *J. Phys. Chem. B* **1997**, *101*, 9027.

(17) Ferrere, S.; Zaban, A.; Gregg, B. A. *J. Phys. Chem. B* **1997**, *101*, 4490.

(18) Ferrere, S.; Gregg, B. A. *J. Am. Chem. Soc*. **1998**, *120*, 843.

(19) Balzani, V.; Campagna, S.; Denti, G.; Juris, A.; Serroni, S.; Venturi, M. *Acc. Chem. Res*. **1998**, *31*, 26.

(20) Usami, A. *Chem. Phys. Lett*. **1997**, *277*, 105.

(21) Ferber, J.; Luther, J. *Sol. Energy Mater. Sol. Cells* **1998**, *54*, 265.

(22) Huang, S. Y.; Schlichthörl, G.; Nozik, A. J.; Grätzel, M.; Frank, A. J. *J. Phys. Chem. B* **1997**, *101*, 2576.

(23) Schlichthörl, G.; Huang, S. Y.; Sprague, J.; Frank, A. J. *J. Phys. Chem. B* **1997**, *101*, 8141.

(24) Kavan, L.; Grätzel, M.; Rathousky, J.; Zukal, A. *J. Electrochem. Soc*. **1996**, *143*, 394.

(25) Papageorgiou, N.; Barbé, C.; Grätzel, M. *J. Phys. Chem. B* **1998**, *102*, 4156.

(26) Schlichthörl, G.; Park, N.-G.; Frank, A. J. *J. Phys. Chem. B* **1999**, *103*, 782.

(27) Dloczik, L.; Ileperuma, O.; Lauermann, I.; Peter, L. M.; Ponomarev, E. A.; Redmond, G.; Shaw, N. J.; Uhlendorf, I. *J. Phys. Chem. B* **1997**, *101*, 10281.

(28) Vanmaekelbergh, D.; Iranzo Marín, F.; van de Lagemaat, J. *Ber. Bunsen-Ges. Phys. Chem.* **1996**, *100*, 616.

(29) de Jongh, P. E.; Vanmaekelbergh, D. *J. Phys. Chem. B* **1997**, *101*, 2716.

(30) Goossens, A.; Boschloo, G. K.; Schooman, L. *Mater. Res. Soc. Symp. Proc*. **1997**, 452 (Advances in Microcrystalline and Nanocrystalline Semiconductors-1996), 607.

(31) Zaban, A.; Ferrere, S.; Sprague, J.; Gregg, B. A. *J. Phys. Chem. B* **1997**, *101*, 55.

(32) Bonhôte, P.; Dias, A.-P.; Papageorgiou, N.; Kalyanasundaram, K.; Grätzel, M. *Inorg. Chem*. **1996**, *35*, 1168.

(33) (a) Matijević, E.; Budnik, M.; Meites, L. *J. Colloid Interface Sci*. **1977**, *61*, 302. (b) Harada, H.; Ueda, T. *Chem. Phys. Lett.* **1984**, *106*, 229.

(34) Cheng, H.; Ma, J.; Zhao, Z.; Qi, L. *Chem. Mater*. **1995**, *7*, 663.

(35) Betsch, R. J.; Park, H. L.; White, W. B. *Mater. Res. Bull*. **1991**, *26*, 613.

(36) Hara, Y.; Nicol, M. *Phys. Status Solidi B* **1979**, *94*, 317.

(37) Balachandran, U.; Eror, N. G. *J. Solid State Chem*. **1982**, *42*, 276.

(38) Porto, S. P. S.; Fleury, P. A.; Daman, T. C. *Phys. Rev*. **1967**, *154*, 522.

(39) Papageorgiou, N.; Grätzel, M.; Infelta, P. P. *Sol. Energy Mater. Sol. Cells* **1996**, *44*, 405.

(40) (a) Munuera, G.; Gonzalez-Elipe, A. R.; Rives-Arnau, V.; Navio, A.; Malet, P.; Soria, J.; Conesa, J. C.; Sanz, J. in *Adsorption and Catalysis on Oxide Surfaces*; Che, M., Bond, G. C., Eds.; Elsevier Science, Amsterdam, 1985; pp 113−126. (b) Lopez, T.; Sanchez, E.; Bosch, P.; Meas, Y.; Gomez, R. *Mater. Chem. Phys*. **1992**, *32*, 141.

(41) Johnson, R. W.; Thiele, E. S.; French, R. H. *Tappi J.* **1997**, *80*, 233.